Journal of Fluids and Structures (2000) **14,** 489–509
doi:10.1006/jfls.1999.0279, available online at http://www.idealibrary.com on IDEAL®

COMPUTATIONAL ANALYSIS OF AEOLIAN CONDUCTOR VIBRATION WITH A STOCKBRIDGE-TYPE DAMPER

J. Vecchiarelli*, I. G. Currie and D. G. Havard†

Department of Mechanical and Industrial Engineering, University of Toronto
5 King's College Road, Toronto, Ontario, Canada M5S 3G8

(Received 27 October 1998, and in final form 4 November 1999)

An iterative finite-difference scheme is derived to predict the vertical, steady-state, monofrequent, aeolian vibration of a single conductor span with a Stockbridge-type damper attached. This numerical scheme is based on empirical models developed to represent the vortex-induced lift force from the wind as well as the forces of dissipation associated with the conductor self-damping and the damper. The scheme has the capability to account for more than one spatial mode of conductor vibration, travelling-wave effects, conductor flexural rigidity, and damper mass. A two-part numerical analysis is performed in which the finite-difference scheme is applied to simulate aeolian vibrations of a typical conductor with and without a Stockbridge-type damper. The computed results are employed to investigate (a) the steady-state form of conductor vibration, (b) the conductor bending amplitudes near each span end as a function of the vibration frequency and damper location, and (c) the influence of conductor flexural rigidity and damper mass. In addition, results from the finite-difference scheme are compared with solutions from the widely used energy balance method as well as field data on aeolian conductor vibrations. The numerical scheme predicts that, with a Stockbridge-type damper attached near a conductor span end, a travelling wave continually propagates towards that span end during steady-state aeolian conductor vibration. It also predicts that, with no dampers attached to a conductor, steady-state aeolian conductor vibration is essentially in the form of a standing wave.

1. INTRODUCTION

Vortex-induced or aeolian vibrations of overhead electrical transmission lines, also referred to as conductors, are very common and can lead to fatigue damage. These vibrations are usually caused by winds ranging in velocity from 1 to 7 m/s and can occur at frequencies from 3 to 150 Hz with peak-to-peak displacement amplitudes of up to one conductor diameter (EPRI, 1979). In conventional transmission line systems, one or more dampers may be attached to a conductor in an effort to suppress aeolian vibrations.

In the present study, the primary objectives are to (i) develop a comprehensive numerical model to determine the steady-state aeolian vibration of a single span of conductor exposed to a steady, uniform crosswind (see Figure 1) and (ii) perform a numerical analysis of the aeolian vibration of a typical conductor using the model and sample damper data. With respect to the first objective, the main intention is to establish a model that is based on the fundamentals of aeolian conductor vibrations and that has the capability of accounting for

* Currently at Atomic Energy of Canada Limited, 2251 Speakman Drive, Mississauga, Ontario, Canada, L5K 1B2
† Currently at Havard Engineering Inc., 3142 Lindenlea Drive, Mississauga, Ontario, Canada, L5C 2C2

0889–9746/00/050489 + 21 $35.00/0

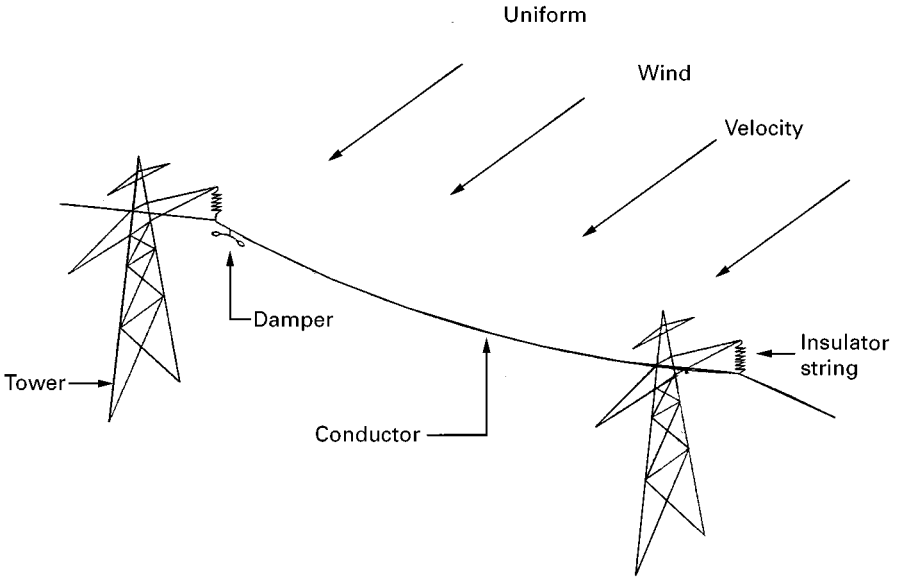

Figure 1. Uniform wind velocity perpendicular to single overhead conductor with damper.

the effects of conductor flexural rigidity, travelling waves, and damper mass. All or some of these effects are usually ignored in many existing models of aeolian conductor vibration. The second objective serves to demonstrate the application of the present model and to investigate the nature of aeolian conductor vibrations. It is noted that the numerical analysis includes a comparison of results from the present model and the widely used energy balance method. In addition, computed results from the present model will be compared to field data on aeolian conductor vibrations.

2. BACKGROUND

Aeolian conductor vibration is influenced by the interaction of: fluid dynamics, conductor self-damping, damper energy dissipation, and conductor dynamics. The aerodynamic and damping forces which act during aeolian vibrations are coupled to the conductor response. An overview of these topics, which are pertinent to the understanding of aeolian conductor vibrations, is provided in Sections 2.1–2.4.

2.1. Conductor Dynamics

The motion of a conductor is governed by Newton's second law. However, a detailed mathematical description of conductor motion is difficult due to the stranded construction of a conductor. The problem is simplified by treating the conductor as a solid, cylindrical body whose physical properties are homogeneous throughout its cross-sectional area (Steidel, 1989). Using this simplification, one can express the governing equation for the transverse or vertical motion of a single conductor in the following dimensionless form (Vecchiarelli *et al.*, 1994)

$$S_p \frac{\partial^4 Y}{\partial X^4} + I_p \frac{\partial^2 Y}{\partial \tau^2} - T_p \frac{\partial^2 Y}{\partial X^2} = \frac{1}{\gamma}\left[F(X,\tau) + \sum_n \delta(X - X_n) F_n(\tau) \right]. \tag{1}$$

In the present study, D represents the conductor diameter, L is the span length, f is the dominant frequency of excitation, m is the conductor mass per unit length, g is the gravitational constant, γ is the conductor weight per unit length (that is, mg), y is the transverse displacement of the conductor relative to its equilibrium or rest position, x is the distance along the conductor, t is time, E is the conductor modulus of elasticity, I is the moment of inertia of the conductor cross-section about the neutral axis, and T is the conductor tension. With respect to equation (1), $Y = y/D$, $X = x/L$, $\tau = t\,f$, $S_p = (EI)D/\gamma L^4$, $I_p = Df^2/g$, and $T_p = TD/\gamma L^2$. Also, $F\ (X,\tau)$ represents the net, transverse force per unit length acting on the conductor, $F_n(\tau)$ represents the nth concentrated force acting transversely on the conductor at the location X_n, and $\delta(X - X_n)$ represents the Dirac delta function (which has units of length^{-1}). The term EI, known as the flexural rigidity, is a measure of conductor stiffness.

In addition to the aforementioned simplification, the following assumptions were made in the derivation of equation (1): (a) the slope of the line tangent to the conductor is small, that is, $\partial y/\partial x \ll 1$, (b) thin beam theory is applicable, and (c) m, T, and EI are uniform across the conductor span. In the present study, the following boundary conditions are assumed: (i) $y = 0$ at $x = 0$, (ii) $y = 0$ at $x = L$, (iii) $\partial y/\partial x = 0$ at $x = 0$, and (iv) $\partial y/\partial x = 0$ at $x = L$. The positions $x = 0$ and $x = L$ correspond to the suspension clamps, that is, the extreme ends of the span. Boundary conditions (i) and (ii) imply that suspension clamps are rigidly fixed. However, it should be noted that suspension clamps have been observed to sway and vibrate (EPRI, 1979). Boundary conditions (iii) and (iv) specify that the conductor is clamped in a horizontal position at each end of the span.

In general, all natural modes will be excited to some extent in the forced response of a continuous system (Bishop & Johnson, 1960), such as a conductor. Furthermore, a conductor can behave very much like a string since the value of flexural rigidity is relatively small.

2.2. Conductor Self-damping

When a conductor flexes, the strands of the conductor slip against each other; this relative motion generates frictional forces that provide damping (Hardy, 1990). In addition, internal losses are incurred at the microscopic level within the core and individual strands of the conductor; this is known as metallurgical or material damping. The combination of these dissipative effects is referred to as conductor self-damping.

Conductor self-damping can be a major source of energy dissipation during aeolian vibrations. However, as conductor tension increases, the strands tend to lock and slippage is reduced. As a result, conductor self-damping decreases and the severity of aeolian vibration increases, thereby raising the potential for fatigue damage. It is for this reason that tensions of undamped conductors are kept relatively low.

Many laboratory studies on conductor self-damping have been performed. The primary focus of these studies was on the energy dissipation due to conductor self-damping. Usually, a sample of a conductor is strung between two rigid terminals and forced to vibrate in one of its natural modes of vibration by means of a shaker. The energy dissipated by the conductor per cycle of vibration is determined (IEEE, 1978) for various tensions, antinodal displacement amplitudes, and frequencies. The determined quantity represents the total energy which is dissipated over the entire test span. Normally, it is possible to represent the experimental results in the following form:

$$\frac{(P_{sd})_r}{L} = K_{sd}\frac{(\hat{y}_a)_r^p f_r^u}{T^v}, \tag{2}$$

where $(P_{sd})_r$ is the average power dissipation due to conductor self-damping, for motion in natural mode r, and it is defined as the total energy dissipated per cycle of vibration divided by the period of vibration, L is the conductor span length, K_{sd} is a constant of proportionality, $(\hat{y}_a)_r$ is the antinodal displacement amplitude corresponding to mode r, f_r is the rth conductor natural frequency, T is the conductor tension, and p, u and v are exponents. Hereinafter, the term amplitude refers to the peak value of a quantity, as opposed to the peak-to-peak value, unless otherwise specified.

Tests on a variety of conductors were carried out by several investigators. The reported values for the exponents in equation (2) typically range as follows (Hardy & Leblond, 1992): 2·0–3·0 for p; 5·0–6·0 for u; and 2·0–3·0 for v. It is emphasized that the determination of the energy dissipated due to conductor self-damping is not straightforward. Significant discrepancies in experimental results can occur as a consequence of extraneous sources of damping, such as aerodynamic resistance.

2.3. Stockbridge-Type Dampers

The Stockbridge damper is presently the most common type of transmission-line damper. In general, a Stockbridge-type damper (Figure 2) consists of two weights attached to the end of stranded cables, which are known as messenger wires. Messenger wires are usually comprised of either 7 or 19 strands of steel and are able to dissipate energy by the same mechanism that a conductor can, that is, through strand slippage and metallurgical damping.

A Stockbridge-type damper is usually placed near a suspension clamp. The general rule followed by transmission-line engineers is to avoid having the damper located at a node, for all expected frequencies of aeolian vibration. The rationale is based on the fact that the damper clamp must experience a finite amount of motion for the damper to dissipate energy. The location of the damper will not coincide with that of a node, for any expected vibration frequency, if the damper is mounted away from the suspension clamp by a distance which is less than the loop length corresponding to the highest expected frequency of vibration. This is reasonable since the conductor loop length increases as the frequency of vibration decreases.

2.4. Fluid Dynamics of Aeolian Vibration

The uniform flow of air or water across a stationary, rigid cylinder whose axis is normal to the streamwise direction has been studied by many investigators; Strouhal (1878) and von Karman (1912) were among the first to do so. Various flow regimes can evolve, depending on the Reynolds number $\mathrm{Re} = \dfrac{VD_{\mathrm{cyl}}}{v}$, where V is the velocity of the fluid, D_{cyl} is the diameter

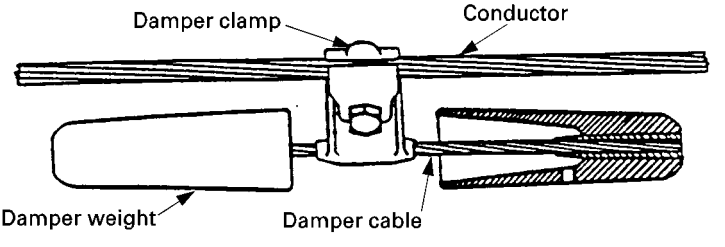

Figure 2. Illustration of Stockbridge-type damper with cross-sectional view of a damper weight.

of the cylinder, and v is the kinematic viscosity of the fluid. Periodic vortex shedding is continuous from Re = 40 to 300 000 (Lienhard 1966). This range of Re includes that which corresponds to light to moderate winds blowing across overhead conductors, for Re based on conductor diameter.

The nature of uniform flow across a rigid cylinder which is mounted on flexible supports is quite different from that of a stationary cylinder. This topic has been explored by numerous investigators, such as Parkinson *et al.* (1968); in-depth reviews are provided by Blevins (1977) and Sarpkaya (1979). Motion of the cylinder in the transverse direction may be initiated when the velocity of the flow is such that the vortex-shedding frequency f_{vs} is close to the natural vibration frequency f_n of the cylinder. The cylinder motion can subsequently (i) increase the strength of the shed vortices, (ii) enhance the spanwise correlation of vortex shedding, and (iii) change f_{vs} to equal or almost equal f_n. The first effect amplifies the magnitudes of the vortex-induced lift forces along the cylinder. The second effect causes these forces to act in phase; that is, they become synchronized (the net lift force which acts on an oscillating cylinder is much greater than that which would exist if the cylinder were stationary). The third effect results in resonance and is referred to as the lock-in phenomenon. As a consequence of these effects, the cylinder may experience a significant level of vibration.

Diana & Falco (1971) measured the lift force that acts during the aeolian vibration of a rigid cylinder in a uniform flow. It was found that, like the displacement of the cylinder, the lift force is virtually harmonic in time at steady state.

Wind-tunnel experiments, in which the wind power input was measured during the aeolian vibration of a circular cylinder, have been performed by many investigators, including: Bate & Callow (1934), Farquharson & McHugh (1956), Diana & Falco (1971), Macdonald *et al.* (1989) and Brika & Laneville (1993). The wind power input is defined as the wind energy transferred to the cylinder over one cycle of vibration divided by the period of vibration. The wind power input per unit length $(P'_w)_{cyl}$ can be expressed in the general form

$$(P'_w)_{cyl} = P\left(\frac{A}{D_{cyl}}, V_r\right) D_{cyl}^4 f^3, \tag{3}$$

where A is the cylinder steady-state displacement amplitude, V_r is the reduced velocity (defined as $V/f_n D_{cyl}$) and $P(A/D_{cyl}, V_r)$ represents a function of A/D_{cyl} and V_r. Differences in the wind power input data from various investigators vary by factors up to 2.

Regarding the aeolian vibration of a flexible cable in a uniform flow, an important conclusion was drawn by Griffin & Ramberg (1974). Based on their wind-tunnel investigation, it was determined that the near wake at a given location along a vibrating cable can be represented reasonably well by the near wake of a rigid cylinder (a) whose diameter is equal to that of the cable and (b) which oscillates at the same frequency and amplitude of the cable at that location. Hence, it may be inferred that the local wind power input along a conductor depends on the local displacement amplitude and frequency of vibration in the same manner that the wind power input for a rigid cylinder depends on the cylinder displacement amplitude and frequency of oscillation. The impact of cable stranding on wind power input is minor (Macdonald *et al.*, 1989).

2.5. The Energy Balance Method

The most widely used methodology for predicting the steady-state aeolian vibration of a conductor is the energy balance method. Mathematically, this method is described as

follows, in terms of power quantities

$$(P_w)_{\text{tot}} = P_{sd} + \sum_n (P_d)_n, \tag{4}$$

where $(P_w)_{\text{tot}}$ is the total wind power input, P_{sd} is the total power dissipated through conductor self-damping, and $(P_d)_n$ is the power dissipated by the nth damper. In the implementation of the energy balance method, a key assumption is that steady-state conductor vibration is in the form of a sinusoidal standing wave of the mode corresponding to the lock-in frequency; refer to CIGRE SC22 WG11 TF1 (2000) and CIGRE SC22 WG01 (1989).

The energy balance method is simple to formulate and is not computationally intensive. However, this method is limited in that it does not account for (i) travelling-wave effects, (ii) contributions from other spatial modes of vibration, (iii) conductor flexural rigidity, and (iv) damper mass.

3. MODEL OF AEOLIAN CONDUCTOR VIBRATION

The particular case of interest in the present study is described as follows (see Figure 1): a single span of conductor exposed to a steady, uniform crosswind that produces vortices at a frequency which coincides with a conductor natural frequency. One or more Stockbridge-type dampers may be attached to the conductor. The conductor is horizontally clamped at both ends of the span by means of suspension clamps. The clamps are assumed to be rigidly fixed. It is also assumed that the suspension clamps are at the same height above ground. Admittedly, the case considered represents an idealization. For instance, field recordings show that aeolian conductor vibrations normally exhibit beating, which indicates the presence of two or more frequencies in the conductor response (EPRI, 1979). Nonetheless, the idealized case is a classic problem of paramount importance in the study of aeolian conductor vibrations.

The present model of aeolian conductor vibration is developed from the fundamentals of conductor dynamics. The model is tailored for the case of monofrequent aeolian conductor vibration. The governing equation of conductor motion is taken to be equation (1). The time dependency of the motion is established *a priori*. This approach substantially reduces the complexity of the problem, as only the spatial component of the motion needs to be solved. The forces due to the wind, conductor self-damping, and Stockbridge-type dampers are modelled based on empirical information.

As mentioned, it is assumed that the wind velocity is uniform and of such a value that the corresponding vortex-shedding frequency exactly matches a natural frequency of the conductor. It is further postulated that lock-in occurs at this frequency along the entire conductor span. From wind-tunnel experiments (Diana & Falco, 1971) on the aeolian vibration of a rigid cylinder in a uniform flow, it is known that the vortex-induced lift force as well as the motion vary harmonically at steady state. Based on this finding and the postulate, it is hypothesized that, during the steady-state aeolian vibration of a conductor in a uniform wind, the local vortex-induced lift force is harmonic in time. From this hypothesis and based on the method of modal analysis, the steady-state conductor displacement is written as follows

$$Y(X,\tau) = Y^*(X)e^{i2\pi\tau}, \tag{5}$$

where $Y^*(X)$ is a complex function representing the spatial component of the steady-state conductor displacement. The actual conductor displacement is given by the imaginary part of the right-hand side of equation (5).

Substitution of equation (5) into equation (1) leads to the following ordinary differential equation:

$$S_p \frac{\mathrm{d}^4 Y^*}{\mathrm{d}X^4} - 4\pi^2 I_p Y^* - T_p \frac{d^2 Y^*}{\mathrm{d}X^2} = \frac{1}{\gamma} \Sigma F^*(\mathrm{X}), \tag{6}$$

where $\Sigma F^*(X)$ is a complex function denoting the sum of the vertical forces that act on the conductor at steady state. For the idealized case, the associated boundary conditions are stated as follows: (i) $Y^* = 0$ at $X = 0$, (ii) $Y^* = 0$ at $X = 1$, (iii) $\mathrm{d}Y^*/\mathrm{d}X = 0$ at $X = 0$, and (iv) $\mathrm{d}Y^*/\mathrm{d}X = 0$ at $X = 1$.

The following describes the modelling of the forces which act during steady-state aeolian vibration of a conductor. The primary forces are: the vortex-induced lift force $F_{vi}(X,\tau)$ associated with the wind, the conductor self-damping force $F_{sd}(X,\tau)$, and one or more damper forces $F_d(\tau)$.

Given the idealized conditions for the case in question in the present study, the model of the steady-state wind force should possess the following characteristics: (i) the wind force varies harmonically in time at the lock-in frequency; (ii) the local energy transferred from the wind force to the conductor equals the wind energy that would be imparted to a rigid cylinder whose diameter is identical to that of the conductor, for the same conditions of aeolian excitation. The first characteristic follows directly from the postulate and the aforementioned hypothesis. The second characteristic is adopted from the energy balance method. This means that the local energy input associated with the vortex-induced lift force has the same functional dependency on the local conductor displacement amplitude as the wind energy input for a rigid cylinder has on the displacement amplitude of the cylinder.

For a given aeolian excitation frequency f of the conductor, characteristic (i) can be satisfied if it is assumed that

$$F_{vi}(X,\tau) = F_w(X)\, \mathrm{e}^{\mathrm{i}2\pi\tau}, \tag{7}$$

where $F_w(X)$ represents the spatial component of the steady-state wind force. The actual wind force is given by the imaginary part of the right-hand side of equation (7). From the basic definition of the local energy transferred per cycle of vibration from the wind force to the conductor, it can be shown that characteristic (ii) is satisfied if

$$F_w(X) = \frac{-E'_w}{\pi \mathrm{D} Y_{Im}(X)}, \tag{8}$$

where E'_w is the local wind energy input for the conductor, determined from wind-tunnel data pertaining to rigid cylinders. For given values of the reduced velocity V_r, f, and D, the quantity E'_w is an explicit function of the dimensionless local displacement amplitude $\hat{Y}$, which depends implicitly on X.

Most of the research in the area of conductor self-damping has involved the acquisition of experimental data on power or energy dissipation. Unfortunately, there is a lack of empirical information pertaining to the conductor self-damping force $F_{sd}(X,\tau)$. However, in a theoretical analysis (Noiseux, 1991), it was hypothesized that this force is of the hysteretic type and that conductor self-damping can therefore be represented in the form of a complex stiffness:

$$EI = EI_o(1 + \mathrm{i}\beta), \tag{9}$$

where EI_o is the flexural rigidity of the undamped conductor, and β is a loss factor.

A suggested form of the conductor self-damping force can be obtained by substituting equation (9) into the governing equation of conductor motion, equation (1):

$$F_{sd}(X,\tau) = -\,\mathrm{i}\,\frac{\beta EI_o D}{L^4}\,\frac{\partial^4 Y}{\partial X^4}. \tag{10}$$

In order for the above equation to be of practical use, a functional relationship must be established between β and the conductor self-damping data for a given conductor. The following requirement is appropriate for the loss factor: the quantity β must be formulated such that the energy loss (over a cycle of vibration) associated with the conductor self-damping force F_{sd} agrees with the experimentally determined value of energy dissipation. To this end, the product of the conductor self-damping force and the conductor velocity is integrated over one period of vibration to obtain a general expression for the local energy dissipated per cycle of vibration (in units of energy per unit length). Then, the local energy dissipation is integrated over the length of the conductor span to yield the following general expression for the total energy dissipated E_{sd} (per cycle of vibration) due to the conductor self-damping force:

$$E_{sd} = \frac{\pi D^2 \beta EI_o}{L^3}\int_0^1 (Y_{\mathrm{Re}} Y''''_{\mathrm{Re}} + Y_{\mathrm{Im}} Y''''_{\mathrm{Im}})\,\mathrm{d}X. \tag{11}$$

The loss factor β for the idealized case of monofrequent aeolian conductor vibration is determined from equation (11) in conjunction with measured values of energy dissipation due to conductor self-damping, for vibration at the mode number corresponding to the lock-in frequency. The energy dissipated is calculated on the basis of the maximum conductor displacement amplitude $\hat{y}_{\max}$.

The force exerted on a conductor by a Stockbridge-type damper effectively acts at a single point. It is assumed that this force acts in the vertical direction. Rotational effects are neglected in the present study; these effects can give rise to horizontal force components as well as moment vectors normal to the vertical plane of conductor vibration (Hagedorn, 1982). As a simplification, any higher harmonic components of a damper force are disregarded. This omission is inherent to the energy balance method and may be justified if the additional harmonics are small relative to the fundamental component of the damper force.

In the present study, a Stockbridge-type damper is modelled as a nonlinear equivalent viscous damper with mass. The vertical force exerted on a conductor by the damper is given by

$$F_d(\tau) = -\,c_d f D\,\frac{\partial Y_d}{\partial \tau} - M_d D f^2\,\frac{\partial^2 Y_d}{\partial \tau^2}, \tag{12}$$

where Y_d is the dimensionless conductor displacement at the location of the damper, c_d is the equivalent viscous damping coefficient, and M_d is a lumped mass.

In general, the equivalent viscous damping coefficient c_d is a function of the vibration frequency f as well as the conductor displacement amplitude $\hat{y}_d$ at the location of the damper clamp. The value of c_d can be determined from measurements of the energy dissipated by a given damper over a complete cycle of vibration of the damper clamp. Damper energy dissipation can be measured via the forced response method (IEEE, 1993), for example. The second term on the right-hand side of the above equation represents an inertial force associated with the damper mass, which can affect the natural frequencies and mode shapes of a conductor. The lumped mass M_d is taken to be the total mass of the damper.

The combination of equation(6) and the four boundary conditions represents a boundary-value problem. For the idealized case of monofrequent aeolian conductor vibration,

solutions entail the application of numerical methods. This is due to the nonlinear nature of the force terms, which consist of the complex spatial components of the wind and damping forces. A finite-difference scheme (Vecchiarelli, 1997) was derived to numerically solve equation(6), subject to boundary conditions (i) through (iv) inclusive. Second-order central differences are employed to replace equation (6) with a pentadiagonal set of algebraic equations for the unknown values of conductor displacement at discrete locations on the span. The integral in equation (11) is evaluated numerically via Simpson's one-third rule, in conjunction with finite-difference expressions for the derivative terms.

In the present study, the nonlinear algebraic equations are solved by means of iteration. For given conditions, a guess is made for the distribution of Y^*. Based on the discrete value of Y^* at each finite-difference node, the forces due to the wind, conductor self-damping, and the damper are evaluated. The linearized algebraic equations are then solved to obtain the updated discrete values of Y^* along the span. This process is iterated until a convergence criterion is satisfied. The iterative procedure has been implemented in a computer program named AEOLUS.

4. NUMERICAL ANALYSIS

4.1. Introduction

As a demonstration of the utilization of AEOLUS, a numerical analysis was carried out for the idealized case of monofrequent aeolian vibration of a 240/40 sq mm ACSR (26/7) conductor (CIGRE SC22 WG11 TF1). The numerical analysis consists of two parts: in Part I, the conductor is without dampers, and in Part II, the conductor features a conventional Stockbridge-type damper. The conductor has the following characteristics: rated tensile strength RTS = 86 400 N, $D = 21{\cdot}9$ mm, and $m = 0{\cdot}987$ kg/m. In the present study, the following span conditions were considered: $T = 17\,280$ N (20% RTS) and $L = 372$ m. The value of T specified is the "everyday" value, that is, the tension at the average temperature of the line over a period of one year. The value of L was selected such that the ratio of conductor sag to span length was 0·026, which is typical of existing transmission lines. It is estimated that the selected conductor also possesses the following characteristics: $EI_{\min} = 16\ \mathrm{N\,m^2}$ and $EI_{\max} = 577\ \mathrm{N\,m^2}$.

The energy-dissipation characteristics (CIGRE SC22 WG11 TF1) of the selected conductor have been determined experimentally for $T = 20\%$ RTS. Based on equation (2), a curve fit of the experimental data was performed. The exponents p and u were calculated to be 2·453 and 5·196, respectively. The curve-fit results are valid only within the following ranges: $10{\cdot}6 \leq f_r \leq 41{\cdot}2$ Hz and $0{\cdot}034 \leq \hat{Y}_{\max} \leq 0{\cdot}528$.

In the present study, the data from the wind-tunnel investigation of Macdonald *et al.* (1989) were used to determine the wind energy input. Based on a regression analysis of the data, a mathematical expression was derived for the wind energy transferred to a rigid cylinder during aeolian vibration. The expression is applicable for a reduced velocity of $V_r \approx 6$ and for $A/D_{\mathrm{cyl}} \leq 0{\cdot}3$. It is noted that, for a given A, the wind energy input decreases as V_r deviates from a value of approximately 6. That is, the maximum wind energy input corresponds to $V_r \approx 6$. Hence, in the present numerical analysis, predictions of conductor displacement correspond to worst-case scenarios. Figure 3 shows a plot of $(E'_w)_{\mathrm{cyl}}/(D_{\mathrm{cyl}})^4(f_{\mathrm{cyl}})^2$ as a function of A/D_{cyl}, based on the empirical expression for wind energy input; here, $(E'_w)_{\mathrm{cyl}}$ is the wind energy input per unit length of cylinder, and f_{cyl} is the vibration frequency of the cylinder. The extrapolated region of the plot indicates that the amount of wind energy input begins to decrease at $A/D_{\mathrm{cyl}} \approx 0{\cdot}5$. Qualitatively, this is consistent with the wind-tunnel data of Diana & Falco (1971). Hence, use of the extrapolated portion of the

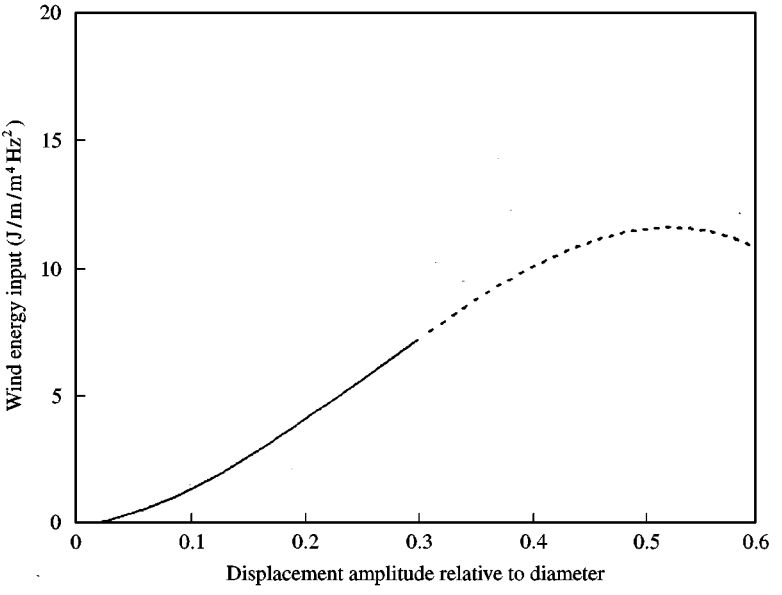

Figure 3. Curve fit of wind energy input data (Macdonald *et al.*, 1989) for a rigid cylinder: – – –, extrapolated data.

curve in Figure 3 may be justified. It is noted that the wind energy input based on the data of Macdonald *et al.* (1989) lies between the upper and lower bounds of all such data that are currently available in the literature. The upper bound corresponds to the data of Diana & Falco (1971), while the lower bound corresponds to the data of Farquharson & McHugh (1956).

During aeolian conductor vibration, alternating bending stresses are created due to the cyclic motion of the conductor. Fatigue failures usually occur at the suspension clamps. The dynamic bending stress at the clamp can be estimated from the measurement of the "bending amplitude" $\hat{y}_b$, which is conventionally defined as the peak-to-peak transverse displacement amplitude at 89 mm (3·5 in) from the last point of contact between the conductor and the suspension clamp. The endurance limit of a conductor is represented in terms of the maximum safe bending amplitude $(\hat{y}_b)_{\text{safe}}$: if $\hat{y}_b$ never exceeds $(\hat{y}_b)_{\text{safe}}$, then it may be assumed that the conductor is safe from fatigue failure. In the numerical analysis, the value of $\hat{y}_b$ at both ends of the conductor span was examined for various frequencies of vibration. For the given conductor with $T = 20\%$ RTS, $(\hat{y}_b)_{\text{safe}}$ is estimated to be 0·316 mm (Lanteigne *et al.*, 1986). In the present study, the value of EI_o was taken to be $EI_{\min}$. This represents a worst-case scenario since the value of the bending amplitude for a conductor with $EI_o = EI_{\max}$ would be less than the corresponding value for the same conductor with $EI_o = EI_{\min}$.

With respect to the implementation of the numerical scheme, the value of the number N of grid points was chosen such that the error associated with the truncation of finite-difference expressions is about 2%. It is emphasized that, in the model of aeolian conductor vibration, additional errors may be incurred due to experimental errors associated with the data used to model the wind, conductor self-damping, and Stockbridge-type dampers. The requisite value of N increases as the dominant mode number and hence vibration frequency increase.

4.2. Results for Part I: Conductor Without Dampers

For the monofrequent aeolian vibration of a conductor without dampers, AEOLUS and the energy balance method yield similar solutions for regions far away from the suspension clamps. These solutions are in the form of standing waves. However, due to the omission of flexural rigidity, the energy balance method overestimates the conductor bending amplitude in the area near a clamp.

In general, the conductor self-damping is small. Thus, with no dampers attached, a conductor should vibrate in a form resembling that of a standing wave, which is the form of vibration assumed in the energy balance approach. Furthermore, since the value of EI_o for a conductor is very small, a conductor tends to behave like a string, which is what a conductor is effectively modelled as in the energy balance method since flexural rigidity is ignored. Hence, with respect to the aeolian vibration of a conductor without dampers, the levels of vibration determined using AEOLUS and the energy balance method should be very close (as confirmed in the present numerical analysis).

On the other hand, the two models give significantly different values of $\hat{y}_b$, for the same f; this can be seen in Figure 4. The energy balance method yields values of $\hat{y}_b$ which are higher than those predicted by AEOLUS. The differences in Figure 4 are attributed to stiffness effects, which tend to reduce the local displacement amplitude near a suspension clamp. Since the energy balance method does not account for flexural rigidity, its predictions of $\hat{y}_b$ are higher than those of AEOLUS, which includes flexural rigidity.

As a general observation, it is also noted that the length of the loop adjacent to the clamp is slightly greater in the AEOLUS solution than it is in the solution from the energy balance method. For example, the difference in loop lengths is estimated to be approximately 40 mm

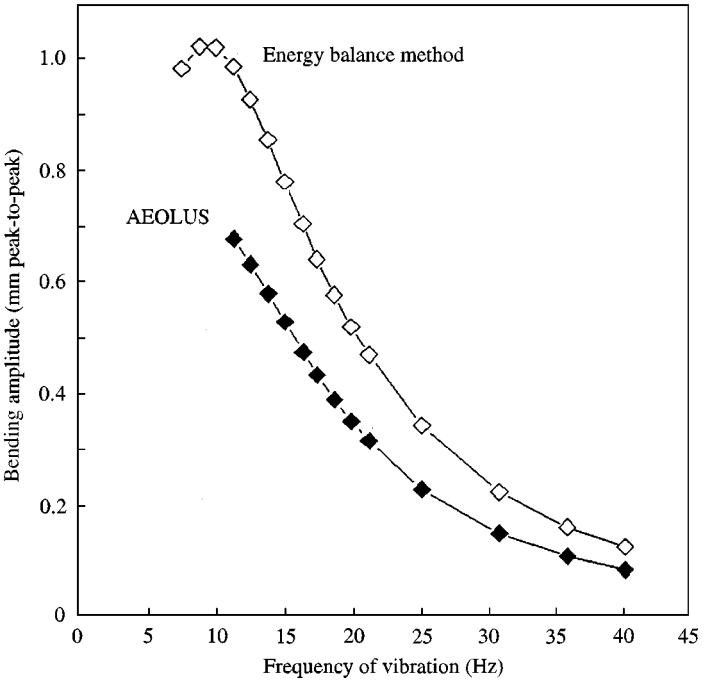

Figure 4. Bending amplitude of 240/40 sq mm ACSR (26/7) conductor as a function of aeolian vibration frequency, based on AEOLUS and energy balance method.

(about 1% relative difference), for the case with $f = 15{\cdot}1$ Hz. This represents another effect of stiffness.

4.3. Results for Part II: Conductor with Damper Attached

In Part II of the numerical analysis, a single Stockbridge-type damper is clamped to the 240/40 sq mm ACSR (26/7) conductor at a relatively short distance x_d from the span end corresponding to $x = 0$. The damper has a mass of $M_d = 4{\cdot}29$ kg and is a symmetrical Stockbridge-type damper. The damping characteristics (Vecchiarelli, 1997) of the damper were experimentally determined by means of the forced response method. The damping data are in the form of energy dissipated per cycle of vibration (of the damper clamp) versus the vibration frequency and displacement amplitude of the damper clamp. The range of applicability of the damper data is specified in terms of the vibration frequency f and the velocity amplitude $2\pi f\,\hat{y}_d$ of the damper clamp. Roughly, the damper data are applicable within the following ranges: $8 \leq f \leq 40$ Hz and $0 \leq 2\pi f\,\hat{y}_d \leq 203$ mm/s.

The form of steady-state conductor vibration typically observed in the AEOLUS solutions is described with reference to the case for which $f = 11{\cdot}4$ Hz and $x_d = 0{\cdot}256$ m. For this reference case, Figure 5 shows the local relative displacement amplitude $\hat{Y}(X)$ of the conductor as a function of distance along the span. It is evident that the values of $\hat{Y}$ are not exactly zero at the nodal points. This indicates that a pure standing wave does not occur.

The true form of conductor motion is best revealed by observing the instantaneous conductor displacement along the span at various moments in time. This is accomplished in Figure 6, which shows the relative conductor displacement during one-tenth of a cycle of vibration, for a 9 m segment of the span. The motion resembles a standing wave in that the antinodal displacement changes from a positive value at a certain location to a negative value at virtually the same location. However, a travelling wave is identified in Figure 6; the wave progresses towards the suspension clamp which is closest to the damper. Moreover, inspection of the AEOLUS results (see Figure 7) for a complete cycle of the conductor vibration (from $\tau = 0$ to $\tau = 1$) leads to the conclusion that: *at steady state, a travelling wave continuously propagates towards the span end which is closest to the damper.*

Physically, the travelling waves are a manifestation of the conductor's endeavor to balance the total wind energy input per cycle of vibration and the total energy dissipated per cycle of vibration. Over most of the span, the local wind energy input exceeds the energy dissipated due to conductor self-damping. As a consequence of this imbalance, energy travels along the span and towards the damper wherein the energy is dissipated. Globally, over the length of the span, the energy input per cycle of vibration matches the energy dissipated per cycle of vibration.

With respect to Figure 6, it is also observed that there is a kink in the conductor at the damper clamp. The kink is associated with the concentrated damping and inertial forces exerted by the damper on the conductor. Figure 6 suggests that the conductor bending stress near the damper clamp may be considerable since the rate of change of the conductor slope with respect to distance along the span appears relatively large.

The presence of the damper has profound effects on the spatial form of conductor vibration. Figure 8 shows the local relative conductor displacement amplitude in the vicinity of the virtual node which is closest to the span end neighboring the Stockbridge-type damper, as computed both with and without the damper mass included. Evidently, the mass of the damper tends to shift the location of the virtual node towards the span end that is closest to the damper; for the reference case, the shift in the nodal point is approximately 93 mm, relative to the location of the nodal point predicted ignoring the mass of the damper. Thus, for the same damper location x_d and $\hat{Y}_{\max}$, the calculated displacement

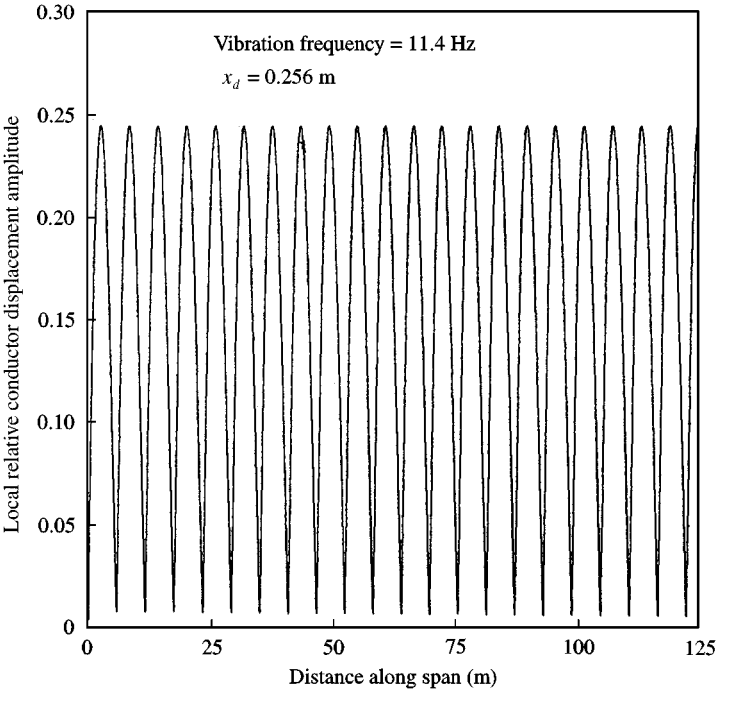

Figure 5. Local relative conductor displacement amplitude $\hat{Y}$ versus distance x along conductor span, as computed with AEOLUS for a vibration frequency f of 11·4 Hz and a damper position x_d of 0·256 m.

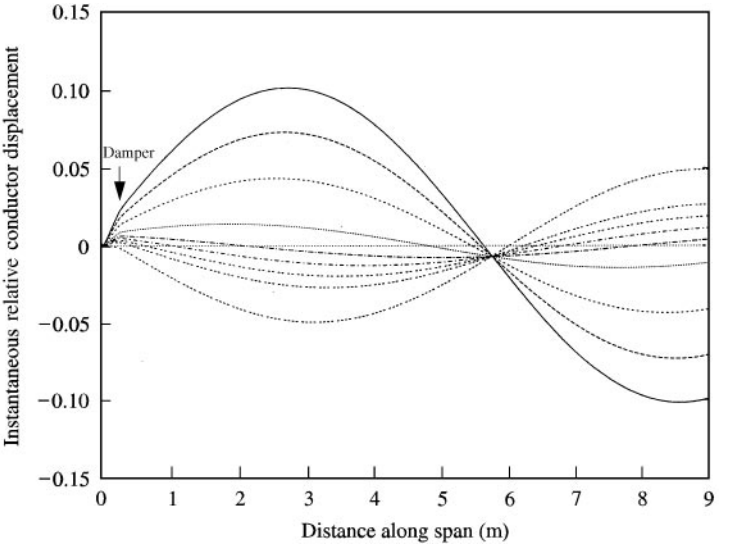

Figure 6. Instantaneous relative conductor displacement Y at various dimensionless times τ within one tenth of a cycle of vibration, as computed with AEOLUS for a vibration frequency f of 11·4 Hz and damper position x_d of 0·256 m: Time: —, 0·000; – – – –, 0·020; -----, 0·040; ....., 0·060; – · – · –, 0·070; - · - · -, 0·075; – – – – – –, 0·080; --- ---, 0·085; -- --, 0·100.

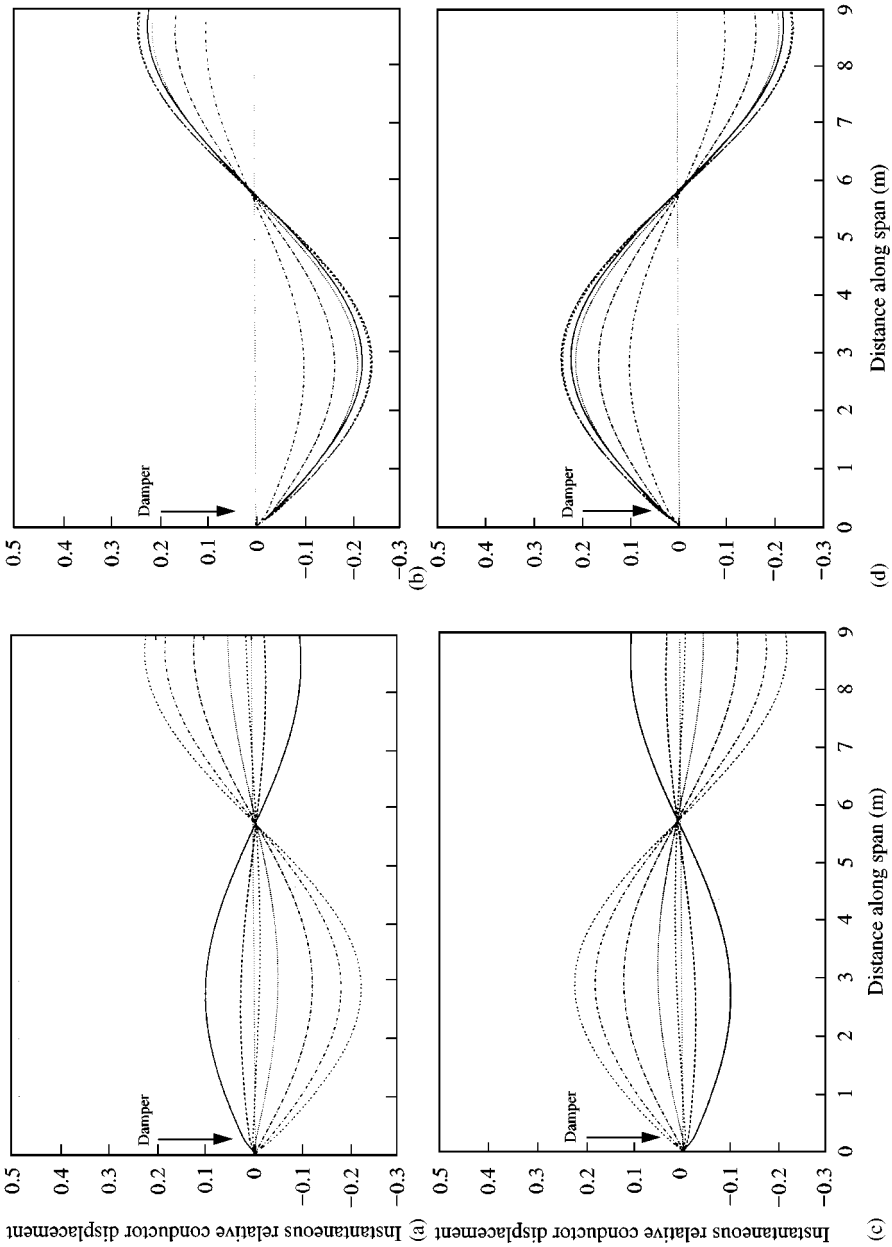

Figure 7. Instantaneous relative conductor displacement Y in region near span end closest to damper, as computed with AEOLUS for a vibration frequency f of 11·4 Hz and damper position x_d of 0·256 m, at various dimensionless times τ between 0 and 1·0: (a) Time: —, 0·000; – – – –, 0·050; – – –, 0·075; ...., 0·100; – · – · –, 0·150; - - - -, 0·200; ……., 0·250; (b) Time: —, 0·25; – – –, 0·30; – – –, 0·35; ...., 0·40; – · – · –, 0·45; - - - -, 0·50; (c) Time: ——, 0·500; – – –, 0·550; – – –, 0·575; ...., 0·600; – · – · –, 0·650; - - - - -, 0·700; ……., 0·750; (d) Time: —, 0·75; – – – –, = 0·80; – – –, 0·85; ...., 0·90; - · - · -, 0·95; - · - · -, 1·00.

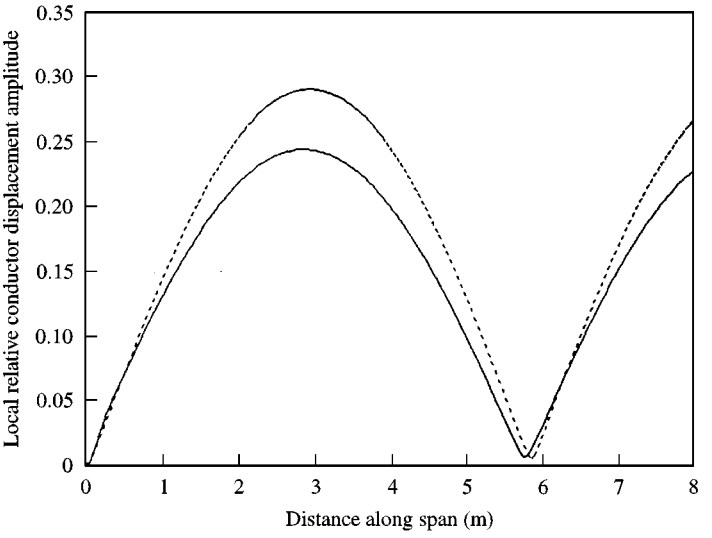

Figure 8. Local relative conductor displacement amplitude in the vicinity of the virtual node closest to damper, as computed using AEOLUS both with and without damper mass M_d included, for a vibration frequency f of 11·4 Hz and damper position x_d of 0·256 m: —, $M_d = 4{\cdot}29$ kg; – – –, $M_d = 0$.

amplitude of the damper clamp is higher when the mass of the damper is included than when the damper mass is neglected. Consequently, since the energy dissipated by the damper increases as the displacement amplitude of the damper clamp increases, the predicted level of aeolian conductor vibration should be generally lower when damper mass is accounted for than when damper mass is ignored. The two solutions in Figure 8 are consistent with this theory.

The form of the steady-state aeolian conductor vibration produced by AEOLUS is markedly different than that assumed in the energy balance method, for the case of a damper attached to the conductor. A key assumption in the energy balance method is that the conductor vibrates in a standing wave. However, the computed results from AEOLUS indicate that travelling-wave effects exist at steady state; that is, a standing wave is not established. Furthermore, the energy balance method assumes a sinusoidal spatial variation for the local conductor displacement amplitude. In the AEOLUS solutions, it is evident that the local conductor displacement amplitude is not purely sinusoidal near the span end which is closest to the damper; in this region, the presence of the damper distorts the conductor displacement profile.

Figure 9 shows values of $\hat{y}_b$ as a function of x_d, as predicted using AEOLUS and the energy balance method for the representative case of $f = 13{\cdot}9$ Hz. The results from the energy balance method apply to the suspension clamps at both ends of the conductor span. That is, the energy balance method yields the same value for $\hat{y}_b$ at the two span ends. This differs qualitatively from the AEOLUS results, which indicate that the two bending amplitudes are generally not the same. Another qualitative difference is that the AEOLUS results indicate an initial increase in the bending amplitude near the span end closest to the damper as x_d increases from zero, whereas the results from the energy balance method show that both bending amplitudes monotonically decrease. These differences in trend are due to the lack of inclusion of damper mass in the energy balance method. In general, the predicted bending amplitude from the energy balance method is significantly greater (typically, at least 25% higher) than that from AEOLUS, for the same x_d. The discrepancies

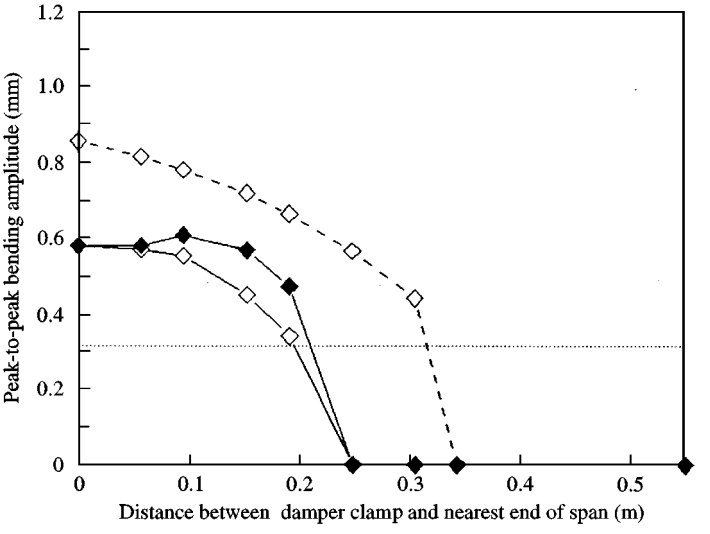

Figure 9. Peak-to-peak bending amplitude $\hat{y}_b$ as a function of distance x_d between damper and nearest end of span, as computed using AEOLUS and the energy balance method, for a vibration frequency f of 13·9 Hz (◆at suspension clamp nearest to damper; ◇ at suspension clamp farthest from damper): ....., maximum safe value; — AEOLUS; – – – energy balance method.

in the values of $\hat{y}_b$ from these two methods are primarily attributable to the effects of conductor stiffness.

The computed results (from both the energy balance method and AEOLUS) in Figure 9 indicate that, for certain x_d values, $\hat{y}_b$ can be reduced to zero. Under the conditions for which $\hat{y}_b = 0$ (and hence $\hat{Y}_{\max} = 0$), the conductor is effectively overdamped. It was determined that, with the damper clamp at certain locations and for any nonzero value of $\hat{Y}_{\max}$, the total wind energy input per cycle of vibration is less than the sum of the energy dissipated by the damper and the conductor. Thus, for these special damper locations, steady-state monofrequent aeolian vibration with a conductor displacement greater than zero is not possible. It is emphasized that this applies to the steady-state phase of aeolian conductor vibration; AEOLUS and the energy balance method do not address the transient phase of conductor motion. It is conceivable that an overdamped conductor would exhibit vibration build-up and decay during aeolian excitation since time is required for wind energy to be transmitted along the span and into the damper. A sustained level of aeolian conductor vibration would not transpire on account of the imbalance between total wind energy input and total energy dissipated by the damper and the conductor. It is noted that $\hat{Y}_{\max}$ will eventually increase from zero as the damper is moved towards the first nodal point corresponding to the vibration frequency.

4.4. Comparison with Field Data

Values of maximum conductor displacement predicted using AEOLUS were compared with measurements obtained during a certain field study. This exercise represents an attempt to assess the validity of the present model of aeolian conductor vibration.

The field study (Diana *et al.*, 1982) took place in Porto Tolle, Italy (near Venice) at a test site located on flat, open terrain near the sea. A 420 kV transmission line extends along this terrain. The transmission line features a bare ACSR (54/19) conductor comprised of 54

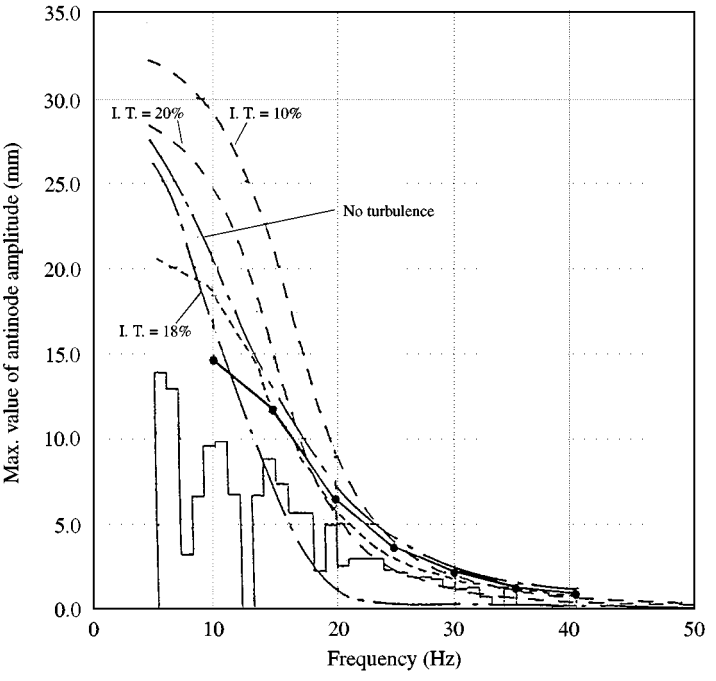

Figure 10. Antinodal conductor displacement amplitude as a function of aeolian vibration frequency, for ACSR (54/19) conductor of span length 453 m and "every day" tension of 34·5 kN, as determined from measurements (Diana *et al.* 1982) and computed using AEOLUS as well as other models (- - - -, – – – –, — · —; I.T. = turbulence intensity): ●—●—●, AEOLUS; —, experimental data.

strands of aluminium and 19 steel strands. The diameter of this conductor is 31·5 mm and the conductor mass per unit length is $m = 1{\cdot}92$ kg/m. A single span of the conductor was employed for the field study; no dampers were attached to the conductor. The length of the selected span is $L = 453$ m. The "every day" conductor tension (at 15°C) was $T = 34500$ N or approximately 20% of the conductor's rated tensile strength RTS. The self-damping properties of the particular type of conductor have been determined from laboratory investigations (Tavano, 1991).

Accelerometers placed near one of the suspension clamps of the span were utilized to estimate the antinodal conductor displacement amplitude in the vertical direction. In addition, the wind velocity was measured at the top of one tower. The duration of the field study was 1·5 months.

Figure 10 shows the experimental values and AEOLUS predictions of the antinodal conductor displacement amplitude as a function of vibration frequency. The computed results from the models of other investigators are also displayed. The experimental data represent the envelope of the measured values of antinodal conductor displacement amplitude. It is observed that the AEOLUS values are greater than the experimental values, for each vibration frequency considered; this is also true for most of the other computed values shown in Figure 10. The discrepancies between the computed and experimental values are not surprising given the many uncertainties in the field study, for example: (i) lock-in may not have occurred at the value of the reduced velocity that results in maximum wind power input (as assumed for AEOLUS), (ii) the wind velocity may not have been steady and uniform along the entire conductor span (as assumed for AEOLUS), (iii) the conductor self-damping data used in AEOLUS may not have accurately represented the damping characteristics of the conductor in the field study, (iv) turbulence levels in the field may

have been considerably higher than the level in the wind tunnel employed to obtain the wind power input data used in AEOLUS, and (v) the measured displacements may have been affected by possible suspension-clamp motion (which is not accounted for in AEOLUS).

The potential sources of error in both the computed and experimental data make it difficult to assess the accuracy of AEOLUS. Nonetheless, it is concluded that the AEOLUS results are qualitatively similar to the measured findings and that the model tends to overestimate the maximum level of aeolian conductor vibration. AEOLUS results for frequencies less than 10 Hz were not attainable, for the given conductor conditions. At such frequencies, computed conductor displacement amplitudes exceeded 50% of the conductor diameter. This caused numerical convergence problems since, beyond a relative displacement amplitude of 0·5, the extrapolated portion of the wind power input curve used in AEOLUS drops rapidly below zero. These numerical difficulties are therefore not inherent to the present approach, rather they are attributable to the nature of the particular wind power input correlation. An alternative correlation may not cause such difficulties. For instance, numerical simulations for frequencies less than 10 Hz were successful when a correlation based on the wind power input data of Diana & Falco (1971) was used in AEOLUS.

It is noted that the AEOLUS values in Figure 10 are generally within the lower and upper bounds of the sets of results from the other investigators, who employed different correlations for the wind power input and conductor self-damping. A sensitivity study (CIGRE SC22 WG11 TF1 2000) indicates that the range of uncertainty in the vibration amplitude predicted via the energy balance method is $\pm$ 50 to 60%, due to uncertainties in the wind power input and conductor self-damping. For comparison, the differences between the antinodal conductor vibration amplitudes predicted by AEOLUS and the energy balance method are significantly less than 50% in the majority of cases considered in the present study.

5. CONCLUSIONS

In the present study, a comprehensive numerical model was derived for the steady-state monofrequent aeolian vibration of a single overhead conductor with a Stockbridge-type damper. The model has the capability of accounting for the effects of: conductor flexural rigidity, more than one spatial mode of conductor vibration, travelling waves, and damper mass. This model is based on empirical data pertaining to wind power input, the conductor self-damping, and the energy-dissipation characteristics of the damper; it is applicable for vibrations in the vertical direction only. The numerical model is implemented in a computer program named AEOLUS.

Based on the computed results from AEOLUS, the primary conclusions from the present study are as follows. In the case of no dampers attached to the conductor span, conductor vibration is essentially in the form of a standing wave during steady-state monofrequent aeolian vibrations. When a Stockbridge damper is located between the first antinodal point and the nearby span end: (i) a travelling wave continually propagates towards the span end which is closest to the damper, and (ii) the damper mass tends to (a) shift the nearby nodal point towards the span end which is closest to the damper and (b) cause a kink in the conductor loop that contains the damper. The energy balance method generally overestimates the bending amplitude at both suspension clamps (due to the omission of conductor flexural rigidity), relative to values predicted using AEOLUS.

These conclusions are meaningful in that they enhance the current understanding of the fundamentals of aeolian conductor vibrations. Some of the conclusions are of practical

significance to transmission-line engineers, while others are of academic interest and are important in their own right.

References

Bate, E. & Callow, J. 1934 The quantitative determination of the energy involved in the vibration of cylinders in an air stream. *Transactions IEE* (*Australia*) **XV,** 149–162.

Bishop, R. E. D. & Johnson, D. C. 1960 *The Mechanics of Vibration.* Cambridge: Cambridge University Press.

Blevins, R. D. 1977 *Flow-Induced Vibrations.* New York: Van Nostrand Reinhold.

Brika, D. & Laneville, A. 1993 Vortex-induced vibrations of a long flexible circular cylinder. *Journal of Fluid Mechanics* **250,** 481–508.

CIGRE SC22 WG01 1989 Report on aeolian vibration. *ELECTRA* No. 124, pp. 41–77.

CIGRE SC22 WG11 TF1 2000 Modelling of aeolian vibrations of single conductors: assessment of the technology. ELECTRA, to be published.

Diana, G. & Falco, M. 1971 On the forces transmitted to a vibrating cylinder by a blowing fluid. *Meccanica* **6,** 9–22.

Diana, G., Gasparetto, M., Tavano, F. & Cosmai, U. 1982 Field measurement and field data processing on conductor vibration: comparison between experimental and analytical results. *CIGRE International Conference on Large High Voltage Electric Systems*, Paper 22–11, Paris, France.

EPRI (Electric Power Research Institute) 1979 *Transmission line reference book*; *wind-induced conductor motion.* Project 792, Palo Alto, California.

Farquharson, F. B. & Mchugh, R. E. 1956 Wind tunnel investigation of conductor vibration with use of rigid models. *Transactions AIEE*, *Power Apparatus and Systems* **75,** 871–878.

Griffin, O. M. & Ramberg, S. E. 1974 Vortex formation in the wake of a vibrating, flexible cable. *ASME Journal of Fluids Engineering* **96,** 317–322.

Hagedorn, P. 1982 On the computation of damped wind-excited vibrations of overhead transmission lines. *Journal of Sound and Vibration* **83,** 879–96.

Hardy, C. 1990 Analysis of self-damping characteristics of stranded cables in transverse vibrations. CSME Mechanical Engineering Forum.

Hardy, C. & Leblond, A. 1992 Comparison of conductor self-damping measurements. CIGRE 1992 General Session, Paris.

IEEE Standard 563–1978 May 1978 *Guide on conductor self-damping measurements.*

IEEE Draft Std. 664–1993 November 3, 1993 *IEEE guide for laboratory measurement of the power dissipation characteristics of aeolian vibration dampers for single conductors.*

Lanteigne, J., Cloutier, L. & Cardou, A. 1986 *Fatigue life of aluminum wires in all aluminum and ACSR conductors.* CEA R&D Project 131 T 241.

Lienhard, J. H. 1966 Synopsis of lift, drag, and vortex frequency data for rigid circular cylinders. Bulletin 300, College of Engineering, Washington State University.

Macdonald, R., Pon, C. J., Havard, D. G. & Currie, I. G. 1989 *Aeolian vibration excitation of Bundle Conductors*, Volumes I and II. Canadian Electrical Association Report, Montreal, Canada.

Noiseux, D. U. 1991 Similarity laws of the internal damping of stranded cables in transverse vibrations. *Proceedings IEEE Transmission and Distribution Conference and Exposition*, Dallas, U.S.A, pp. 817–823.

Parkinson, G. V., Feng, C. C. & Ferguson, N. 1968 Mechanisms of vortex-excited oscillation of bluff cylinders. *Symposium on Wind Effects on Buildings and Structures*, Loughborough University of Technology, Paper No. 27.1.

Sarpkaya, T. 1979 Vortex-induced oscillations: a selective review. *Journal of Applied Mechanics* **46,** 241–258.

Steidel, Jr., R. F. 1989 *An Introduction to Mechanical Vibrations*, 3rd Edition. New York: John Wiley & Sons.

Strouhal, V. 1878 Über eine besondere Art der Tonerregung. *Annalen der Physik und Chemie*, New Series, Vol. **5,** 216–251.

Tavano, F. 1991 *Collection of experimental data on aeolian vibration on single conductors.* CIGRE 22–91 (WG 11-TF1) 6.

Vecchiarelli, J. 1997 Aeolian vibration of a conductor with a Stockbridge-type damper. Ph.D. Thesis, University of Toronto, Canada.

VECCHIARELLI, J., CURRIE, I. G. & HAVARD, D. G. 1994 A proposed numerical analysis of aeolian conductor vibrations. *Proceedings of the* 12*th Symposium on Engineering Applications of Mechanics*: *Interactions of Fluids*, *Structures and Mechanisms*, McGill University, Montreal, Quebec, Canada, pp. 225–234.

VON KÁRMÁN, T. 1912 Über den Mechanismus des Widerstandes, den ein bewegter Körper in einer Flüssigkeit erfärt, Göttinger Nachrichten, mathematisch-physikalische Klasse, 509–517, 1911; 547–556, 1912.

APPENDIX: NOMENCLATURE

A	steady-state displacement amplitude of cylinder
c_d	equivalent viscous damping coefficient of Stockbridge-type damper
D	diameter of conductor
D_{cyl}	diameter of cylinder
E	conductor modulus of elasticity
EI	conductor flexural rigidity ($E \times I$)
$EI_{\max}$	maximum value of EI
$EI_{\min}$	minimum value of EI
EI_o	undamped flexural rigidity of conductor
E_{sd}	total energy dissipated due to conductor self-damping
E'_w	wind energy input per unit length of conductor
$(E'_w)_{\text{cyl}}$	wind energy input per unit length of cylinder
f	frequency of conductor vibration (Hz)
f_{cyl}	frequency of vibration of cylinder (Hz)
f_n	natural frequency of vibration of cylinder (Hz)
f_r	conductor natural frequency corresponding to mode r (Hz)
f_{vs}	vortex-shedding frequency (Hz)
$F(X,\tau)$	same as $F(x,t)$
$\sum F^*(X)$	sum of the complex spatial components of all applied forces
$F_d(\tau)$	force from damper
$F_n(\tau)$	vertical, concentrated force at $X = X_n$
$F_{sd}(X,\tau)$	conductor self-damping force
$F_{vi}(X,\tau)$	vortex-induced lift force associated with the wind
$F_w(X)$	spatial component of wind force
g	gravitational constant
I	conductor cross-sectional moment of inertia about neutral axis
I_p	dimensionless inertia parameter (Df^2/g)
K_{sd}	constant of proportionality associated with conductor self-damping
L	conductor span length
m	conductor mass per unit length
M_d	total mass of Stockbridge-type damper
n	positive integer
N	number of finite-difference nodes between conductor span terminals
p	exponent associated with conductor self-damping
$P(A/D_{\text{cyl}},V_r)$	function associated with wind power input for cylinder
$(P_d)_n$	power dissipated by nth damper
P_{sd}	power dissipated due to conductor self-damping
$(P_{sd})_r$	power dissipated due to conductor self-damping, for standing-wave vibration in mode r
$(P'_w)_{\text{cyl}}$	cylinder wind power input per unit length
$(P_w)_{\text{tot}}$	total wind power input for conductor
r	mode number (integer)
Re	Reynolds number
RTS	rated tensile strength of conductor
S_p	dimensionless stiffness parameter ($EI \cdot D/\gamma L^4$)
t	time
T	conductor tension
T_p	dimensionless tension parameter ($T \cdot D/\gamma L^2$)
u	exponent associated with conductor self-damping

v	exponent associated with conductor self-damping
V	velocity of fluid
V_r	reduced velocity
x	distance along conductor span
x_d	value of x at location of damper
X	x/L
X_n	value of X at location denoted by n
$y(x,t)$	vertical displacement of conductor
$\hat{y}(x)$	local displacement amplitude of conductor
$(\hat{y}_a)_r$	conductor antinodal displacement amplitude corresponding to mode r
y_b	conductor bending amplitude
$(\hat{y}_b)_{\mathrm{safe}}$	maximum safe bending amplitude of conductor
y_d	value of y at location of damper
$\hat{y}_d$	displacement amplitude of conductor at location of damper
$\hat{y}_{\max}$	maximum value of y
$Y(X,t)$	y/D
$\hat{Y}$	$\hat{y}/D$
$Y^*(X)$	$Y/\mathrm{e}^{\mathrm{i}2\pi\tau}$
Y_d	y_d/D
$Y_{\mathrm{Im}}(X)$	imaginary component of $Y^*(X)$
$\hat{Y}_{\max}$	maximum value of $\hat{Y}$
$Y_{\mathrm{Re}}(X)$	real component of $Y^*(X)$
β	loss factor associated with conductor self-damping
γ	conductor weight per unit length
δ	Dirac delta function
ν	kinematic viscosity of fluid
τ	dimensionless time (tf)